Optics Letters

Femtosecond laser-ablation of gel and water

Javier Hernandez-Rueda,[1,2,3,†] Dashdeleg Baasanjav,[1,†] Allard P. Mosk,[1] and Dries van Oosten[1,*]

[1]Debye Institute for NanoMaterials Science and Center for Extreme Matter and Emergent Phenomena, Utrecht University, Princetonplein 5, 3584 CC Utrecht, The Netherlands
[2]Kavli Institute of Nanoscience Delft, Department of Quantum Nanoscience, Delft University of Technology, Lorentzweg 1, 2628 CJ Delft, The Netherlands
[3]e-mail: fjavihr@gmail.com
*Corresponding author: d.vanoosten@uu.nl

Received 14 February 2020; revised 16 April 2020; accepted 28 April 2020; posted 29 April 2020 (Doc. ID 390506); published 28 May 2020

We study the expansion dynamics of super-heated material during ultra-fast laser ablation of water and gel, using transient-reflectivity microscopy. We find that the expansion dynamics of water and gel, as observed during the first few nanoseconds, are extremely similar over a large range of ablation energies. We measure the crater topography of the gel after irradiation with a single laser shot, using optical interferometric microscopy, and estimate the mass that is ejected during the ablation. We calculate the laser energy deposited during irradiation by simulating the precise spatial distribution of the electron plasma density and temperature. We link the amount of removed mass obtained experimentally with the simulations of the deposited laser energy.

https://doi.org/10.1364/OL.390506

The advent of femtosecond (fs) laser amplification has, over the last three decades, enabled the study of the interaction of extremely intense light fields with dielectric materials. Many of these studies focused on the use of the above-mentioned interaction to produce permanent material changes, which gave rise to the field of fs-laser micromachining of transparent materials [1–4], half way between the fields of photonics and materials science. Similarly, permanent fs-laser-induced changes have singularly important applications in the field of laser-based surgery, i.e., neurosurgery and ocular surgery [5–10]. A key problem in laser-tissue interactions is the so-called photomechanical damage that results from the conversion of light energy into mechanical energy [11–13]. Light-tissue interactions are very complicated to model and so understanding the physical mechanisms that mediate the interaction of intense ultrashort laser pulses with water is crucial, since water is the main constituent of biological tissue.

Laser-water interactions have extensively been studied, with nanosecond [14–16], picosecond [16,17], and femtosecond laser pulses [18–22]. Here, it is of paramount importance to realize (1) the different laser energy absorption mechanisms and (2) the time-scales in which absorption occurs. For short (pico- to nanosecond) pulses the energy is absorbed mainly through the excitation of impurities in water, and later on via avalanche ionization [23]. Once the laser creates a plasma it keeps supplying energy to that plasma up to several picoseconds or nanoseconds, which means that the super-heated material expands while the laser field is still present. For ultrashort laser pulses the energy absorption is mediated via strong field ionization (i.e., multiphoton and tunneling ionization) and avalanche ionization [24–27], similarly to the situation in a transparent solid target [28–33]. In this case, the energy deposition is ultrafast, which leads to a distinct separation in time of the energy deposition (<1 ps) and the material expansion onset (50 ps-1 ns) [18,22]. This separation helps to compartmentalize the problem. Recently, our group reported on a model that explains the laser-induced electron plasma properties in water during the first picosecond. The model simultaneously accounts for laser pulse propagation and nonlinear energy absorption considering a dynamically evolving dielectric function of excited water, which is validated using the experimentally acquired transient reflectively [27]. It therefore provides an estimate of the spatial distribution of the deposited energy. The expansion dynamics is also quite well studied (mainly for longer pulses as explained above), but information about ejected water mass is hard to obtain due to the lack of an aftermath.

In this work, we use single femtosecond laser pulses to investigate laser ablation of water and a porcine-based gel. Using time-resolved microscopy we link distinct features of the material expansion during the nanosecond time-scale. This comparison enables us to establish a correspondence between the ultrafast laser ablation in gel and water. Furthermore, the use of the gel specimen has two clear benefits, it is a better tissue phantom than water is, and it provides a measure of the ejected mass that is estimated by measuring the volume of the single-laser-shot-generated craters. We use model calculations [27], to estimate the energy that is deposited using different laser fluences and compare it to the ejected mass.

The experimental procedure is shown in Fig. 1. To prepare the gel sample, we mix 1.5 g of gelatin from porcine gel (G2625-100 G Sigma-Aldrich) with 15 ml of mili-Q demineralized water at a temperature of approximately 50°C, after which we pour 3 ml of the hot gel mixture into a plastic container with

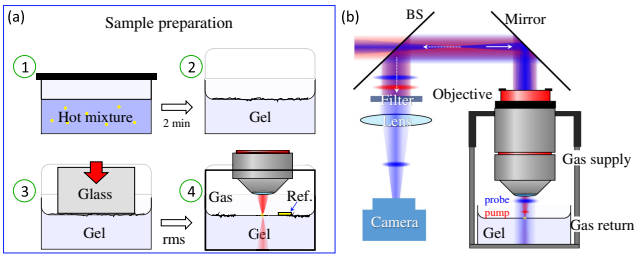

Fig. 1. (a) To prepare gel samples with a sufficiently flat surface, the gel is mixed (1) and allowed to partially set (2), after which an optical flat is gently dropped onto the surface (3). After the gel has fully set the optical flat is removed. A marker (Ref) is placed on the surface of the gel, and the sample is mounted in the ablation setup (4). (b) The gel sample is mounted in a cuvette, such that the composition of the gas above the gel can be controlled. The gel is illuminated by a focused pump pulse (depicted in red) and a wide-field probe pulse (depicted in blue). The reflection from the probe is used to image the surface on a CCD camera.

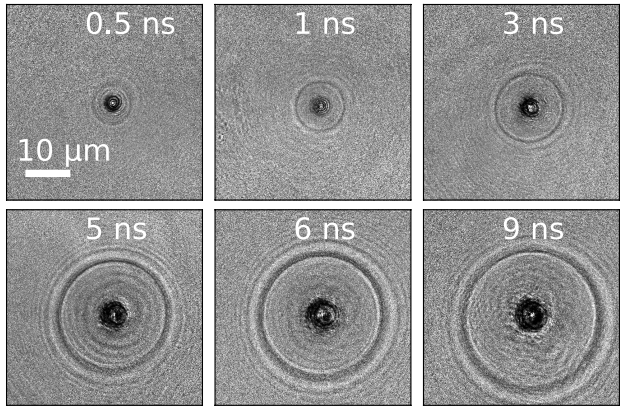

Fig. 2. Transient reflectivity images obtained at several pump-probe delays, during the ablation of gel in an atmosphere of tetrafluorethane. We clearly note a dark disk in the center, with a ring-shaped feature centered around it. The laser energy per pulse was set to be 5 μJ, corresponding to a fluence of 27.5 J/cm^2.

a 2 cm diameter. We allow the gel to partially set, waiting for 5 minutes at room temperature, after which we gently place a polished fused silica glass substrate ($\lambda/20$) onto the gel surface, as illustrated in Fig. 1(a). After the gel has fully set, we remove the glass substrate, leaving a small and flat surface (1 cm^2) suitable for ablation experiments. The optical experiments are carried out in the transient reflectivity microscope, previously described in Ref. [21] and summarized in Fig. 1(b). Single femtosecond laser pulses from an amplified Ti:Sapphire laser are focused on the gel surface using a microscope objective. Using the Liu method [34], the beam waist on the surface is determined to be 3.4 μm. The laser pulse duration is 150 fs (full width half-maximum) and the central laser wavelength 800 nm. The objective and the gel are enclosed in a container that allows us to control the atmosphere above the gel. Part of the light from the laser is split off and frequency doubled. These much weaker pulses are delayed using an optical delay line and then also sent through the objective. The reflection from this probe light is imaged using a camera as a function of pump-probe delay. Typical results of such measurements are shown in Fig. 2, which were carried out above a gel surface. We interpret the dark disk in the center of this images as the ablation plume that propels upwards, towards the objective. The ring-shaped feature that can be seen concentrically around the disk appears to be associated with a shock-wave in the surrounding atmosphere, as the radius and the strength of the features at a given pulse energy and pump-probe delay can be strongly influenced by changing the composition of the background gas. For the measurements shown here, the background gas was tetrafluorethane (TFE), which produces a particularly strong ring. We attribute this to the fact that the sound velocity in TFE is only ≈168 m/s, which is very small compared to the observed radial expansion velocity of the ring (≈810 m/s [22]). When air is used as a background gas, the ring is much weaker and when Helium is used, no ring can be observed for the pulse energies used here. An exact study of the behavior of the ring is, however, outside of the scope of this work.

Water and gel are to some extent expected to behave similarly under ablation condition; they have comparable mass densities of 1.00 g/cm^3 and 1.10 g/cm^3, respectively. Furthermore, the gel has a refractive index of 1.36–1.38 [35,36], which is close to that of water. Also, linear optical absorption of both water and gel is negligible at the pump wavelength. However, the nonlinear optical properties of the gel are largely unknown. To compare water and gel, we therefore determine the radius of the black disk and the ring by performing an azimuthal average of each image, measured at a fixed pump-probe delay of 10 ns and as a function of the incident pulse energy. The result of this analysis is shown in Fig. 3. The blue symbols in the graph correspond to the radius of the black disk and the orange symbols to the radius of the ring. The differences in properties of water and gel apparently have only a minor influence on the expansion of the ablation plume, as we clearly see that there is no significant difference between the behavior of those features when measured on gel (closed symbols) or water (open symbols). This strongly suggests that the ablation behavior of gel and water are also very similar in this energy range. Crucially this means that we can combine what we can learn from gel with what we already know about water, as we will do in the following. In particular, this means that we can estimate the amount of material that is ablated (in either water or gel) by measuring the surface topography of the gel after ablation. Material can be removed by thermal processes and non-thermal processes, such as Coulomb explosion (CE). As explained in the review [2], CE typically removes material up to a depth of a few nanometers, under conditions where the total ablation depth is on the order of a few ten nanometers per pulse. We therefore expect thermal processes to be dominant under our conditions. We measure the surface topography of the gel using an optical profilometer. Typical results of such measurements are shown in Fig. 4. The top row shows topography maps of two ablation craters created by a single laser pulse with energies of 5.0 μJ [Fig. 4(a)] and 2.5 μJ [Fig. 4(b)], corresponding to fluences of 27.5 J/cm^2 and 13.8 J/cm^2, respectively. Note that these maps contain some roughness around the crater (caused by the initial surface roughness), which limit the accuracy of the measurements discussed below. The bottom row shows the associated azimuthal averages. From these averages, we can obtain the depth of the crater (measured from the bottom of the crater to the top of the rim), the radius (which we define as the width measured halfway between the bottom of the crater to

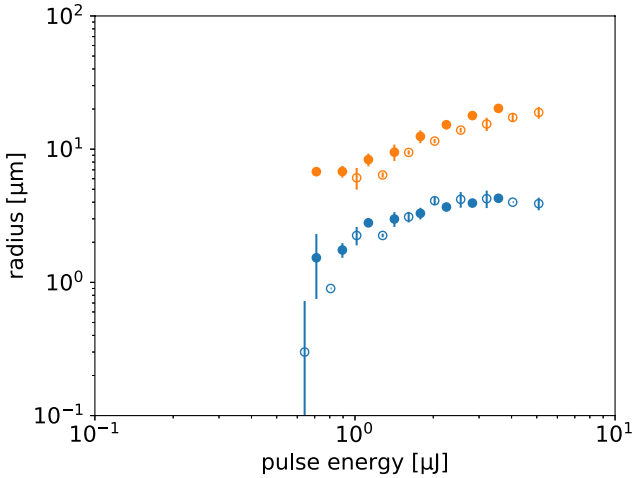

Fig. 3. This graph compares the radii of modification of water (open symbols) and gel (closed symbols), measured at a pump-probe delay of 10 ns. The blue symbols correspond to the radius of the dark disk, the orange symbols to the radius of the ring-shaped feature.

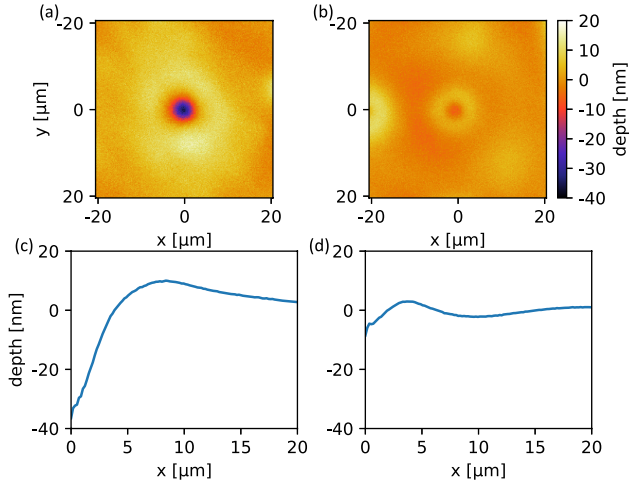

Fig. 4. Surface topography of the gel after (a) strong and (b) gentle ablation, obtained using optical profilometry. The bottom panels (c) and (d) show corresponding azimuthal averages around the center of the ablation craters.

the top of the rim) and the crater volume (which we define as the volume inside the radius).

The results of this analysis are shown in Fig. 5. The top graph shows the depth (blue points, left y-axis) and the radius (orange points, right y-axis) as a function of the incident pulse energy. The error bars are the standard deviation taken over up to three craters created using the same pulse energy. The bottom graph shows the estimate of the removed volume (blue points, left y-axis). The volume seems to show a subtle threshold behavior around an incident pulse energy of 2.5 µJ (incident fluence 13.8 J/cm^2), although we should be careful not to attach too much value to that single data point. It should be pointed out that the first data point that shows a measurable crater volume is at 1.55 µJ, corresponding to a fluence of 8.5 J/cm^2. This is comparable to the threshold fluence of 8.1 J/cm^2 which we

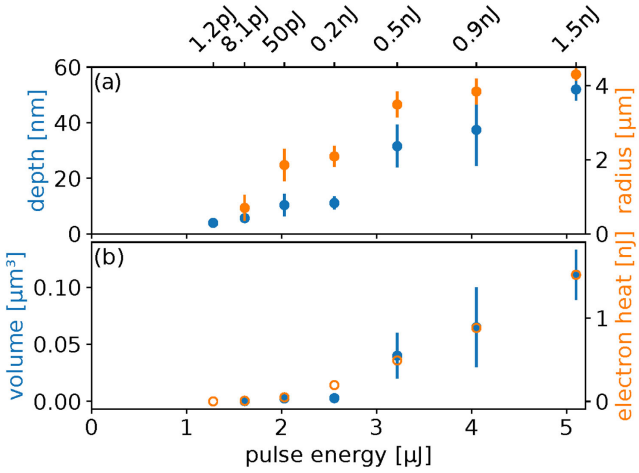

Fig. 5. (a) Crater depth (blue symbols, left axis) and radius (orange symbols, right axis) as a function of incident pulse energy. (b) Crater volume (solid blue symbols, left axis) and the electron heat as obtained from model calculations (open orange symbols, right axis) as a function of incident pulse energy.

estimated for water on the basis of the apparent evaporation onset [22].

As we have argued above, the behavior of gel and water appear sufficiently similar to combine what we can learn from experiments on the ablation of gel with what we already understand about the ablation of water. We therefore use our previously established finite-difference-time-domain model for the ablation of water [27] to compute energy that is absorbed by the water for each of the experimentally used incident pulse energies. Specifically, we compute the part of the energy that is stored in the form of the heat of the resulting electron plasma. These energies are indicated as the ticks on the top x-axis and also shown in the bottom graph (orange circles, right y-axis). Note that the scale of the right y-axis is chosen such that the electron heat for that pulse energy coincides with the average measured crater volume.

Remarkably, the measured volume and the computed electron heat show a strikingly similar dependence on the incident pulse energy. In fact, the overlap is fortuitously good, given the error bars. Thus, under the conditions of our experiment, the ablation plume has a specific energy that seems almost independent of incident pulse energy. In Ref. [37], it is shown that for silica, the expansion velocity of the ablation plume is only weakly dependent on the pulse energy. Interestingly our results for water and gel are consistent with a plume expansion velocity that is independent of pulse energy. If we subtract from this specific energy the latent heat of evaporation and assume the remainder is used as kinetic energy of the plume, we find a velocity for the plume of 5 ± 1 km/s for the three energies above the apparent threshold at 2.5 µJ. As this number is highly supersonic, it is likely that most of the energy is initially converted into vertical kinetic energy.

It is as of yet unclear to us why the effective velocity we find would be independent of, or at least insensitive to, the incident pulse energy. Furthermore, we currently do not know what determines this velocity. One could argue that it should be related to the sound velocity in the super-critical and highly

ionized material in the ablation zone. Yet this sound velocity is hard to obtain independently.

In conclusion, we have shown that the ablation plume dynamics of water and aqueous gel are extremely similar. We have used this similarity to combine aftermath results of the ablation of gel with numerical models established to describe the absorption of ultra-short laser pulses by water. This has allowed us to estimate the initial velocity of the ablation plume, which is surprisingly insensitive to the absorbed laser energy. This surprising feature could in the future be studied further, possibly combined with side-view imaging or other methods.

Funding. H2020 Marie Skłodowska-Curie Actions (703696 ADMEP); Nederlandse Organisatie voor Wetenschappelijk Onderzoek (VICI 68047618).

Acknowledgment. The authors thank Cees de Kok, Paul Jurrius, and Dante Killian for technical support.

Disclosures. The authors declare no conflicts of interest.

[†]These authors contributed equally to this work.

REFERENCES

1. R. R. Gattass and E. Mazur, Nat. Photonics **2**, 219 (2008).
2. P. Balling and J. Schou, Rep. Prog. Phys. **76**, 036502 (2013).
3. L. Englert, B. Rethfeld, L. Haag, M. Wollenhaupt, C. Sarpe-Tudoran, and T. Baumert, Opt. Express **15**, 17855 (2007).
4. J. Hernandez-Rueda, J. Clarijs, D. van Oosten, and D. M. Krol, Appl. Phys. Lett. **110**, 161109 (2017).
5. M. F. Yanik, H. Cinar, H. N. Cinar, A. D. Chisholm, Y. Jin, and A. Ben-Yakar, Nature **432**, 822 (2004).
6. A. Vogel, J. Noack, G. Hüttman, and G. Paltauf, Appl. Phys. B **81**, 1015 (2005).
7. M. H. Niemz, *Laser-Tissue Interactions*, 4th ed. (Springer, 2007).
8. H. A. Collins, M. Khurana, E. H. Moriyama, A. Mariampillai, E. Dahlstedt, M. Balaz, M. K. Kuimova, M. Drobizhev, V. X. D. Yang, D. Phillips, A. Rebane, B. C. Wilson, and H. L. Anderson, Nat. Photonics **2**, 420 (2008).
9. S. X. Guo, F. Bourgeois, T. Chokshi, N. J. Durr, M. A. Hilliard, N. Chronis, and A. Ben-Yakar, Nat. Methods **5**, 531 (2008).
10. Z. Nagy, A. Takacs, T. Filkorn, and M. Sarayba, J. Refract. Surg. **25**, 1053 (2009).
11. R. R. Krueger, J. S. Krasinski, C. Radzewicz, K. G. Stonecipher, and J. J. Rowsey, Cornea **12**, 330 (1993).
12. G. Paltauf and H. Schmidt-Kloiber, Appl. Phys. A **68**, 525 (1999).
13. C. P. Cain, C. A. Toth, G. D. Noojin, D. J. Stolarski, R. J. Thomas, and B. A. Rockwell, Heal. Phys. **82**, 855 (2002).
14. A. L. Klein, W. Bouwhuis, C. W. Visser, H. Lhuissier, C. Sun, J. H. Snoeijer, E. Villermaux, D. Lohse, and H. Gelderblom, Phys. Rev. Appl. **3**, 44018 (2015).
15. X. Zeng, X. Mao, S. S. Mao, S.-B. Wen, R. Greif, and R. E. Russo, Appl. Phys. Lett. **88**, 061502 (2006).
16. A. Vogel, S. Busch, and U. Parlitz, J. Acoust. Soc. Am. **100**, 148 (1996).
17. T. Juhasz, X. H. Hu, L. Turi, and Z. Bor, Lasers Surg. Med. **15**, 91 (1994).
18. C. B. Schaffer, N. Nishimura, E. N. Glezer, A. M.-T. Kim, and E. Mazur, Opt. Express **10**, 196 (2002).
19. C. Sarpe-Tudoran, A. Assion, M. Wollenhaupt, M. Winter, and T. Baumert, Appl. Phys. Lett. **88**, 261109 (2006).
20. B. D. Strycker, M. M. Springer, A. J. Traverso, A. A. Kolomenskii, G. W. Kattawar, and A. V. Sokolov, Opt. Express **21**, 23772 (2013).
21. M. Vreugdenhil, D. van Oosten, and J. Hernandez-Rueda, Opt. Lett. **43**, 4899 (2018).
22. J. Hernandez-Rueda and D. van Oosten, arXiv:1810.06946 (2018).
23. A. Vogel, Phys. Med. Biol. **42**, 895 (1997).
24. C. Sarpe, J. Köhler, T. Winkler, M. Wollenhaupt, and T. Baumert, New J. Phys. **14**, 075021 (2012).
25. N. Linz, S. Freidank, X.-X. Liang, H. Vogelmann, T. Trickl, and A. Vogel, Phys. Rev. B **91**, 134114 (2015).
26. T. Winkler, C. Sarpe, L. L. H. N. Jelzow, N. Götte, B. Zielinski, P. Balling, A. Senftleben, and T. Baumert, Appl. Surf. Sci. **374**, 235 (2016).
27. J. Hernandez-Rueda and D. van Oosten, Opt. Lett. **44**, 1856 (2019).
28. L. V. Keldysh, Sov. Phys. JETP **20**, 1307 (1965).
29. B. Rethfeld, Phys. Rev. Lett. **92**, 187401 (2004).
30. V. E. Gruzdev, Phys. Rev. B **75**, 205106 (2007).
31. B. Rethfeld, Phys. Rev. B **73**, 035101 (2006).
32. B. Christensen and P. Balling, Phys. Rev. B **79**, 155424 (2009).
33. J. Hernandez-Rueda, D. Puerto, J. Siegel, M. Galvan-Sosa, and J. Solis, Appl. Surf. Sci. **258**, 9389 (2012).
34. J. M. Liu, Opt. Lett. **7**, 196 (1982).
35. A. J. Durkin, S. Jaikumar, and R. Richards-Kortum, Appl. Spectrosc. **47**, 2114 (1993).
36. H. G. Akarçay, S. Preisser, M. Frenz, and J. Rička, Biomed. Opt. Express **3**, 418 (2012).
37. E. Axente, S. Noöl, J. Hermann, M. Sentis, and I. N. Mihailescu, J. Phys. D **41**, 105216 (2008).